PHYSICAL REVIEW A

GENERAL PHYSICS

THIRD SERIES, VOLUME 27, NUMBER 5 MAY 1983

Relaxation calculation of the electrostatic properties of compensated Penning traps with hyperbolic electrodes

Gerald Gabrielse

Department of Physics, FM-15, University of Washington, Seattle, Washington 98195

(Received 27 December 1982)

Spectacular accuracies have been achieved with single elementary particles trapped in hyperbolic Penning traps, but only after anharmonicities have been tuned out of these traps by varying the potential of extra compensation electrodes introduced into the traps. The relaxation calculation reported here is the first theoretical study of the electrostatic properties of such compensated Penning traps. Enough computations have been completed to clarify the basic physics involved in anharmonicity compensation and to provide useful, quantitative information for experiments in progress (especially for testing of anharmonicity systematics). The clearer picture of anharmonicity compensation which emerges suggests that the design of existing Penning traps could be significantly improved. An optimal electrode configuration is proposed which, in principle, makes the harmonic oscillation frequency of a trapped particle independent of changes in the compensation potential.

I. INTRODUCTION

A single electron was first trapped in a Penning trap at the University of Washington.[1] Subsequent progress[2] led to measurements of the magnetic moments of both the electron[3] and the positron[4] to accuracies of 5×10^{-11}. The measurements of the magnetic-moment anomalies are the most stringent tests of quantum electrodynamics which has recently been used to calculate the anomalies to the order α^4 (in Ref. 5). Comparison of the electron and positron magnetic moments provides an unprecedented test of the invariance of the electron-positron system under *CPT*. Experiments are now underway whose ultimate goals are to trap a single proton[6] (in order to measure the proton-electron mass ratio) and to improve the accuracy of the magnetic moment of the electron to 10^{-12} or better.[7] All of these experiments are only possible when anharmonicities are tuned out of the Penning traps by adjusting the potential on extra compensation electrodes introduced into the traps.

Although extra electrodes were included in an earlier trap to improve the trapping potential produced by nonhyperbolic electrodes,[8] the first dramatic decrease in the anharmonicity of a precision, hyperbolic Penning trap was reported in Ref. 9. In that report the first compensated trap and a slight variation on it (with pointed compensation electrodes) were discussed. Subsequently, the first compensated trap was used for electron anomaly measurements,[3] and essentially, identical copies of the second were used for positron measurements[4] and to observe the relativistic mass increase of a 0.5-eV electron.[7] These traps were so successful that no great effort was expended to systematically study electrostatic anharmonicity.

Penning traps constructed more recently for the proton experiments[6] and for next-generation $g-2$ measurements[7] led to an increased appreciation of the severity of the electrostatic screening involved in anharmonicity compensation. However, attempts to improve the ability of Penning traps to tune out anharmonicities without shifting the harmonic-oscillation frequency of a trapped particle were not very successful. The time required to design, construct, and assemble a precision hyperbolic trap (typically a year or more) and the difficulty involved in making precise measurements of their electrostatic properties obstructed progress towards such an

optimized trap.

The relaxation calculation reported here speeds up the process a great deal. In fact, initial calculations which were carried out in just several weeks were already very useful for making trap-building decisions. Over the last year, when time allowed, a variety of configurations of hyperbolic Penning traps with different compensation geometries was examined. For each configuration, the relatively small number of parameters of importance for particle trapping (discussed in Sec. II) were calculated. The recent availability of an array processor greatly facilitated these calculations. Section III describes the relaxation calculation itself, including an important coordinate transformation used to avoid mismodeling the hyperbolic electrodes.

Enough computations have now been completed to provide a clearer picture of the basic physics involved in anharmonicity compensation and to provide useful quantitative information for experiments in progress (especially for testing for systematic effects of electrostatic anharmonicities). Section IV focuses on a particular choice of hyperbolic electrodes (labeled as an asymptotically symmetric Penning trap). The existing compensated traps are all asymptotically symmetric traps. The lessons learned in the study of such traps make clear that the design of existing Penning traps could be significantly improved. Section V summarizes the successful search for an optimized configuration of hyperbolic electrodes. Section VI is a conclusion.

The calculation applies to a compensated Penning trap with electrodes that are perfectly aligned and are free of holes, slits, or imperfections. While the effects of harmonic distortions of the potential and stray homogeneous electric fields (together with misalignments of the magnetic field) have been shown in an earlier paper to be completely avoidable,[10] imperfections and misalignments do modify some of the quantities calculated in this paper as do holes and slits in electrodes. Fortunately, changes in the trapping potential which result from a change in the compensation potential are not greatly modified by these complications. The few measurements available from high-precision traps agree very well with the calculation.

II. COMPENSATED PENNING TRAPS

An ideal Penning trap consists of a homogeneous magnetic field (taken to be in the $\hat{z}$ direction) together with two hyperbolic endcap electrodes and one hyperbolic ring electrode, all of which are axially symmetric about the z axis. The endcap and ring electrodes lie along the contours

$$z^2=z_0^2+\tfrac{1}{2}\rho^2 \tag{2.1}$$

and

$$z^2=-\tfrac{1}{2}\rho_0^2+\tfrac{1}{2}\rho^2\,, \tag{2.2}$$

respectively, where ρ and z are cylindrical coordinates. The constants ρ_0 and z_0 are thus the minimum radial and axial distances to the ring and endcap electrodes from the center of the trap. Whatever the values of ρ_0 and z_0, the electrodes asymptotically approach the cones $z^2=\frac{1}{2}\rho^2$ for large ρ and z.

For endcaps at potential $\frac{1}{2}V_0$ and ring at $-\frac{1}{2}V_0$, the ideal electrodes produce the potential

$$V_{\text{ideal}}=V_0C(\rho_0/z_0)+V_0\frac{z^2-\frac{1}{2}\rho^2}{z_0^2+\frac{1}{2}\rho_0^2}\,. \tag{2.3}$$

The first term on the right is an unobservable constant [which will, however, be used in Eq. (2.15)] given by

$$C(\rho_0/z_0)=-\frac{1}{2}\frac{z_0^2-\frac{1}{2}\rho_0^2}{z_0^2+\frac{1}{2}\rho_0^2}\,. \tag{2.4}$$

The second term is the desired quadrupole potential for a Penning trap. Notice that both ρ and z are naturally scaled in the potential by a characteristic trap dimensional d given by

$$d^2=\tfrac{1}{2}(z_0^2+\tfrac{1}{2}\rho_0^2)\,. \tag{2.5}$$

For the most popular choice of $\rho_0=\sqrt{2}z_0$, the endcap and ring electrodes approach the asymptotic cones symmetrically for large ρ and z. We thus call this configuration an asymptotically symmetric Penning trap and observe that $d=z_0$ and $C(\rho_0/z_0)$ vanishes for this special case.

The potential in a laboratory Penning trap V deviates from the potential for the ideal trap with the same ρ_0 and z_0 by ΔV,

$$V=V_{\text{ideal}}+\Delta V\,. \tag{2.6}$$

The deviation is due to holes and slits in the quadrupole electrodes (to admit particles and various radio-frequency and microwave drives) together with imperfections, misalignments, and truncations of these electrodes. In a compensated Penning trap, extra compensation electrodes introduced into the asymptotic region[11] contribute to ΔV and allow ΔV to be changed. Figure 1 is a scale drawing of a laboratory Penning trap with hyperbolic electrodes. Figure 2 shows the model electrodes used for the relaxation calculation of Sec. III. The compensation electrode is symmetric about the asymptote and characterized by the angle α. Notice that $\alpha=180°$ is a flat

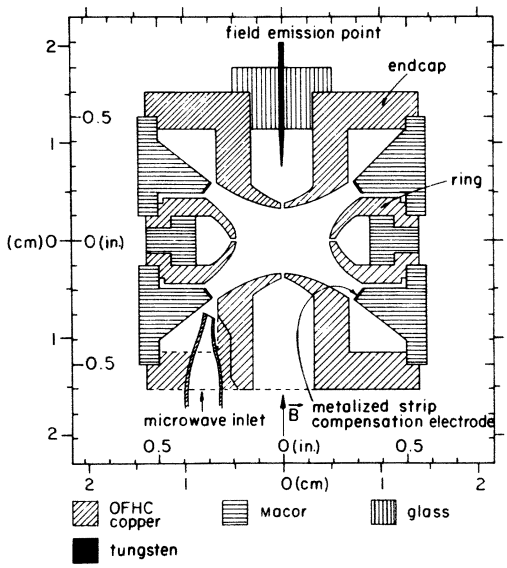

FIG. 1. Drawing of the most recently constructed compensated Penning trap. It was designed by the author and is currently being used in an attempt to measure an electron's magnetic moment to an accuracy of 10^{-12}. Drawing is to scale except for the holes in the endcaps and the slit in the ring which are slightly enlarged to make them visible. Electrodes are axially symmetric about the magnetic field vector shown.

electrode perpendicular to the asymptote, while $\alpha=0°$ is a compensation electrode which lies entirely on the asymptote.

For particle trapping, complete knowledge of ΔV is not required since particles are typically trapped near the center of the trap where the spherical coordinate $r \ll d$. In this region [at position (r,θ,ϕ) in spherical coordinates] ΔV can be conveniently expanded in a familiar way in even-order Legendre polynomials $P_k(\cos\theta)$ multiplied by r^k,

$$\Delta V = \tfrac{1}{2} V_0 \sum_{\substack{k=0, \\ \text{even}}} C_k \left[\frac{r}{d}\right]^k P_k(\cos\theta) \, . \tag{2.7}$$

The compensation electrodes, holes and slits in electrodes, truncations, etc., which produce $\Delta V \neq 0$ are assumed here to maintain axial symmetry about the z axis and reflection symmetry under $z \rightarrow -z$. As demonstrated in Fig. 1, these symmetries are carefully maintained in the construction of precision Penning traps. Distances in Eq. (2.7) are scaled by the characteristic trap dimension.

As mentioned, only the lowest-order coefficients are important for particle trapping. The first, C_0, is unobservable and can be ignored. The major effect of $C_2 \neq 0$ is an amplitude-independent shift of the harmonic-oscillation frequency ω_z of a trapped particle of charge q and mass m (from the harmonic-oscillation frequency of an ideal trap with the same ρ_0 and z_0),

$$\omega_z^2 = \frac{qV_0}{md^2}(1+C_2) \, . \tag{2.8}$$

A $C_4 \neq 0$ produces highly undesirable shifts (in the three eigenfrequencies of the trapped particle) which depend upon oscillation amplitudes. Most important is the shift of the axial frequency $\Delta\omega_z$ which results from an energy E_z in the axial oscillation,[12]

$$\frac{\Delta\omega_z}{\omega_z} \approx \tfrac{3}{2} C_4 \frac{E_z}{qV_0} \, . \tag{2.9}$$

A factor of $(1+C_2)^{-2}$ has been neglected on the right since $C_2 \ll 1$ for a good trap. Even when the trapped particle is driven weakly enough so that no drive-related anharmonicity shift is observed, thermal excitations of the axial motion broaden the axis resonance width. In experiments so far, the axial motion has been coupled to a damping resistor at temperature T_z which is at or somewhat above the bath temperature, depending upon whether or not the detection electronics is off or on. To roughly estimate the resulting linewidth, consider a Boltzmann distribution of axial excitation energies E_z at temperature T_z. The root-mean-squared spread in excitation energies is equal to kT_z. Thus a rms axial linewidth Γ_z roughly given by

$$\frac{\Gamma_z}{\omega_z} \approx \tfrac{3}{2} |C_4| \frac{kT_z}{qV_0} \tag{2.10}$$

results from electrostatic anharmonicity. This anharmonicity linewidth must be added in quadra-

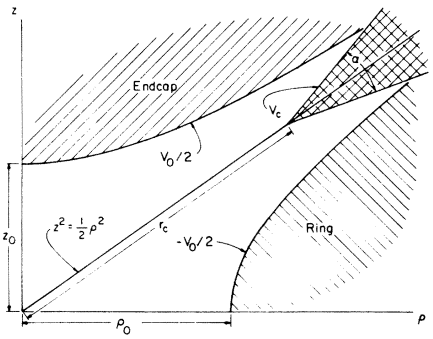

FIG. 2. Model used for calculating the electrostatic potential in a hyperbolic Penning trap. Relaxation calculations are carried out for various α and r_c as well as for various ratios for ρ_0 to z_0. Endcap, ring, and compensation electrodes are at $\frac{1}{2}V_0$, $-\frac{1}{2}V_0$, and V_c, respectively. The particular example shown is an asymptotically symmetric trap with $\alpha=30°$ and $r_c/d \approx 2.2$.

ture to other contributing linewidths to produce the total observed linewidth. Measured axial linewidths thus provide an estimate (or upper limit) for $|C_4|$. Uncompensated traps have been built[13] with $|C_4|<10^{-2}$ and more recently[14] with $|C_4|<10^{-3}$. The compensated traps reported in Ref. 9 have produced $|\tilde{C}_4|<10^{-4}$ when carefully tuned.[15]

The coefficient C_4 quantifies the major part of trap anharmonicity and therefore will dominate the discussion in the rest of this paper. Other C_k can also contribute slightly, however, especially when C_4 is reduced a great deal by tuning the compensation potential. The most likely contributors are C_6 from Eq. (2.7) and C_3 which is not included in Eq. (2.7) because it vanishes when reflection symmetry is perfectly maintained. The axial frequency shift in Eq. (2.9), for example, acquires additional terms which can be accounted for by replacing C_4 [in Eq. (2.9)] by

$$\tilde{C}_4 \approx C_4 - \tfrac{5}{4}C_3^2 + \tfrac{5}{2}C_6\frac{E_z}{qV_0} . \tag{2.11}$$

The odd-order coefficient C_3 enters as the square because it is associated with an odd-parity term in the potential which can perturb energy levels only in second order. Higher-order coefficients like C_6 are of higher order in E_z/qV_0. This ratio is typically of order 10^{-4} for $E_z \approx kT_z$. The additional terms thus should produce a small offset from C_4 and a small dependence upon E_z which can be detected typically only after C_4 is reduced by tuning the compensation potential.

To compensate trap anharmonicities, the potential V_c of the compensation electrodes is tuned to minimize the observed width of the axial resonance and/or to minimize drive-dependent shifts of ω_z and thus to minimize C_4.[9] The potential coefficients C_k are linear in this compensation potential. To see this, observe that the boundary conditions for V in Fig. 2 are the superposition of the boundary conditions in Figs. 3(a) and 3(b) which uniquely determine solutions to Laplace's equation, ϕ_0 and ϕ_c, respectively, so that

$$V = V_0\phi_0 + V_c\phi_c . \tag{2.12}$$

Both V_{ideal} and the expansion of ΔV are explicitly linear in V_0 but not in V_c. Thus each C_k is the sum of a term which is independent of V_c and a term linear in V_c/V_0,

$$C_k = C_k^{(0)} + \left[V_0\frac{dC_k}{dV_c}\right]\frac{V_c}{V_0} . \tag{2.13}$$

The $C_k^{(0)}$ pertain to a compensation potential $V_c=0$ which is midway between the endcap and ring potentials. A nonzero compensation potential adds a second term which can be used to cancel the first and thus eliminate a troublesome C_k, typically C_4. It is important to notice that the dimensionless constants $V_0 dC_k/dV_c$ are actually independent of V_0, V_c, and d. We label these quantities the tunabilities for C_k since they represent a trap's ability to tune out C_k.

From Eq. (2.12) it is evident that only two solutions of Laplace's equation are required to completely specify the potential in a flawless, compensated Penning trap for all possible values of V_0, V_c, and d.

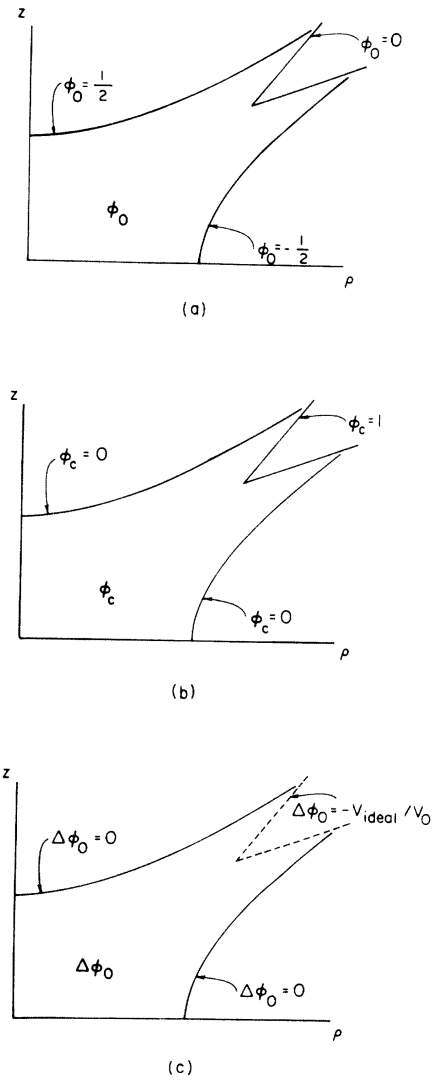

FIG. 3. Boundary conditions which together with axial symmetry about the z axis and reflection symmetry under $z \rightarrow -z$ define the solutions to Laplace's equation: ϕ_0 in (a), ϕ_c in (b), and $\Delta\phi_0$ in (c).

The tunabilities $V_0 dC_k/dV_c$ can be determined solely from ϕ_c. Observe from Eq. (2.12) that ϕ_c is equal to dV/dV_c. Since V_{ideal} is independent of V_c, differentiating the expansion for ΔV with respect to V_c yields

$$\phi_c = \frac{1}{2} \sum_{\substack{k=0, \\ \text{even}}}^{\infty} \left[V_0 \frac{dC_k}{dV_c} \right] \left[\frac{r}{d} \right]^k P_k(\cos\theta) . \quad (2.14)$$

The tunabilities (first term in large parentheses) are the expansion coefficients for ϕ_c. Equivalently, the tunability for C_k is a kth-order derivative of ϕ_c in the limit that r goes to zero. The $C_k^{(0)}$ can be obtained solely and most directly from a new solution to Laplace's equation

$$\Delta\phi_0 = \phi_0 - V_{\text{ideal}}/V_0 , \quad (2.15)$$

which we use in place of ϕ_0. The boundary conditions for $\Delta\phi_0$ [in Fig. 3(c)] include ring and endcap boundaries at $\Delta\phi_0 = 0$. The compensation electrode boundary is dashed in Fig. 3(c) since it varies from $-\frac{1}{2}$ at the endcap to $+\frac{1}{2}$ at the ring. At each point on this boundary $\Delta\phi_0$ is equal to $-V_{\text{ideal}}/V_0$. Combining Eqs. (2.6), (2.7), and (2.12) for the special case $V_c = 0$ yields

$$\Delta\phi_0 = \frac{1}{2} \sum_{\substack{k=0, \\ \text{even}}}^{\infty} C_k^{(0)} \left[\frac{r}{d} \right]^k P_k(\cos\theta) . \quad (2.16)$$

The $C_k^{(0)}$ are thus the expansion coefficients for $\Delta\phi_0$.

Both $\Delta\phi_0$ and ϕ_c vanish on the endcap and ring boundaries. The boundaries for these two solutions [in Figs. 3(c) and 3(b)] thus differ only (but significantly) on the compensation electrode boundary. On this boundary, $\Delta\phi_0$ varies from $\Delta\phi_0 = -\frac{1}{2}$ at the endcap end to $\Delta\phi_0 = \frac{1}{2}$ at the ring end, while ϕ_c is an equipotential at $\phi_c = 1$. The substantial dipole character of $\Delta\phi_0$ on the compensation boundary (as viewed from the center of the trap), by contrast to the monopole character of ϕ_c on the same boundary, typically makes $\Delta\phi_0$ much smaller than ϕ_c near the center of the trap. This means that the $C_k^{(0)}$ which are important for particle trapping are typically smaller in magnitude than the corresponding $V_0 dC_k/dV_c$, since these are exact counterparts in the expansions for $\Delta\phi_0$ and ϕ_c, respectively. Thus according to Eq. (2.13), C_4 can be made to vanish with a compensation potential V_c which is smaller in magnitude than the trapping potential V_0, for a flawless trap.

The hyperbolic electrodes of a laboratory Penning trap often contain small holes and slits to admit particles and various radio-frequency and microwave drives. We shall not attempt to calculate the effect of holes and slits here, since a different technique is required. We observe, however, that holes and slits in the hyperbolic electrodes would primarily modify the boundary conditions which determine $\Delta\phi_0$. The additional contributions to $C_k^{(0)}$ make it difficult to precisely estimate the net $C_k^{(0)}$ for a laboratory trap. In a good trap, however, the $C_k^{(0)}$ can easily be made much less than 1 as evidenced by the $|C_4| \approx 10^{-2}$ to 10^{-3} realized in uncompensated traps. Fortunately, ϕ_c near the center of the trap (and hence tunabilities like $V_0 dC_4/dV_c$) is much less modified by the addition of holes, slits, imperfections, and misalignments. Measured values of $V_0 dC_2/dV_c$, in fact, agree very well with the calculated values. We shall focus upon the tunabilities since a trap must be designed to ensure an adequate value of $V_0 dC_4/dV_c$.

A clear and direct test of the relaxation calculation is possible because the tunability for C_2 can be simply and directly measured. From Eq. (2.8)

$$V_0 \frac{dC_2}{dV_c} = \frac{2V_0}{\omega_z} \frac{d\omega_z}{dV_c} . \quad (2.17)$$

A factor of $(1+C_2)^{-1}$ has been approximated as 1 on the left since $C_2 \ll 1$ for a good trap. Measurements of the change in the harmonic-oscillation frequency as a function of the compensation potential thus constitute a test of the relaxation calculation. Several such measurements are plotted later (in Fig. 8). The significance of $V_0 dC_2/dV_c$ for trap design is more readily apparent when the factor $\omega_z/2V_0$ in Eq. (2.17) is identified as $d\omega_z/dV_0$ so that

$$V_0 \frac{dC_2}{dV_c} = \frac{d\omega_z/dV_c}{d\omega_z/dV_0} . \quad (2.18)$$

The axial frequency can be changed by varying either the trapping potential V_0 or the compensation potential V_c. For the precision electron, positron, and proton experiments mentioned, standard cells are used for V_0 to provide a sufficiently stable and noise-free axial frequency ω_z. Less stability is therefore required in the compensation potential V_c than in the trapping potential V_0 by a factor of the tunability for C_2 according to Eq. (2.18).

It is clearly desirable to design the trap electrodes to make $V_0 dC_2/dV_c$ much less than 1 so that a lesser quality, variable potential source can be used for V_c. At the same time, the electrodes must be designed to make $V_0 dC_4/dV_c$ large enough so that C_4 can be made to vanish with a reasonable compensation potential. To qualify this additional consideration for trap design we define a quality factor γ for precision Penning traps,

$$\gamma = \frac{V_0 dC_2/dV_c}{V_0 dC_4/dV_c} . \quad (2.19)$$

A minimum $|\gamma|$ is most desirable, since γ

represents the undesirably axial frequency shift which accompanies an adjustment of C_4 by a particular amount as can be seen from the equivalent definition,

$$\gamma=\frac{2}{\Delta C_4}\frac{\Delta\omega_z}{\omega_z}\ . \tag{2.20}$$

Both $\Delta\omega_z$ and ΔC_4 are brought about by a small change in the compensation potential. The relaxation calculation shows that $\gamma\approx 0.56$ for all of the existing electron, positron, and proton traps—completely independent of innovations in compensation electrode shape and location. This is not at all optimal. We show in Sec. V that γ can, in principle, be made to vanish. In practice, however, a reduction of γ by a factor of 20 seems feasible, though no such trap has yet been constructed.

The quality factor γ is also important for a calibration of $V_0 dC_4/dV_c$. This tunability cannot be so easily measured as can the tunability for C_2. The quality factor relates these two tunabilities and according to the relaxation calculation is often nearly independent of the shape and location of the compensation electrodes. Thus a value

$$\frac{V_0 dC_4}{dV_c}\simeq\frac{1}{\gamma}\frac{d\omega_z/dV_c}{d\omega_z/dV_0} \tag{2.21}$$

may be inferred from measurements of the change in ω_z brought about by changes in V_c and V_0. The electrostatic anharmonicity coefficient C_4 can thus be varied by well-known amounts to test for systematic effects of anharmonicity.

The sign of $V_0 dC_4/dV_c$ can be more directly measured by driving the axial oscillation to a very high oscillation energy E_z. The classical anharmonic oscillation which results is well understood, being completely discussed, for example, in Ref. 12. Observe from Eq. (2.9) that $d\omega_z/dE_z$ and C_4 have the same sign since the well depth qV_0 must be positive if a particle is to be trapped. Thus from Ref. 12 we deduce that the axial resonance line shape is sharply cut off on the high-frequency side for $C_4>0$ and on the low-frequency side for $C_4<0$ as illustrated in Fig 4. Varying V_c establishes the sign of $V_0 dC_4/dV_c$. A value $V_0 dC_4/dV_c<0$ is measured and calculated for the existing compensated traps, all of which are asymptotically symmetric traps.

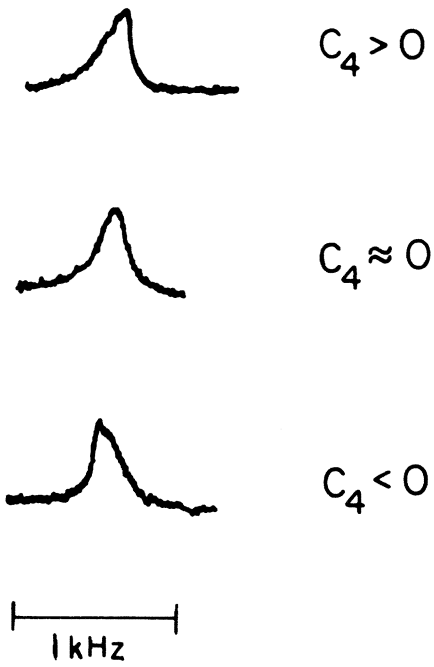

FIG. 4. Axial resonance line shapes for a cloud of ($\approx$30) electrons trapped in the compensated Penning trap of Fig. 1. The center profile represents a compensation potential which is tuned so that $C_4\approx 0$. Increasing and decreasing the compensation potential produces the characteristic skewed resonance shapes for $C_4>0$ (above) and $C_4<0$ (below).

III. RELAXATION CALCULATION

In a region bounded by fixed potentials, any solution to Laplace's equation which satisfies the boundary conditions is the unique electrostatic potential. The iterative, relaxation technique is a convenient way to find this unique solution when a "good guess" at the solution is available as it is for a high-quality Penning trap. The interior of the trap is covered with an appropriate grid of discrete mesh points. Laplace's equation provides an expression for evaluating the potential at a particular mesh point in terms of potentials at neighboring mesh points. For the simplest case of mesh points equally spaced in rectangular coordinates, for example, the potential at each point is just the average of the potentials of its six nearest neighbors plus corrections of order of the mesh spacing h to the fourth power. Each point is so evaluated in terms of its neighbors, over and over again until successive iterations produce negligible changes in the potential, which is then determined uniquely to order h^4. The starting estimate of the potential determines how many iterations are necessary before the potential converges.

The electrodes of a laboratory Penning trap (e.g., Fig. 1) completely bound the three-dimensional interior of the trap with fixed potentials, except for small gaps between the electrodes which we shall model as negligibly small as indicated in Fig. 2. The electrodes additionally are axially symmetric about the z axis and are symmetric under reflections

$z \rightarrow -z$. These symmetries make it advantageous to switch to cylindrical coordinates to reduce the three-dimensional trap volume to an area within a single quadrant as shown in Figs. 2 and 3 and thereby bring about a considerable reduction in the number of mesh points which are required. This savings comes at the expense of a slightly more complicated version of Laplace's equation

$$0=\frac{\partial^2 V}{\partial z^2}+\frac{\partial^2 V}{\partial \rho^2}+\frac{1}{\rho}\frac{\partial V}{\partial \rho}\ , \tag{3.1}$$

which differs from Laplace's equation in two dimensions by the addition of the last term. Relaxation formulas for mesh points equally spaced in ρ and z are correspondingly more complicated than the simple averaging mentioned earlier for mesh points spaced evenly in rectangular coordinates. Notice in Fig. 2 that portions of the $\hat{\rho}$ and $\hat{z}$ axes serve as boundaries. These boundaries are not equipotentials, of course, but are bounded by the appropriate reflection and/or axial symmetry enforced on these boundaries.

We transform further from cylindrical coordinates to coordinates

$$t=z^2-\tfrac{1}{2}\rho^2\ , \tag{3.2}$$

$$s=z^2+\tfrac{1}{2}\rho^2\ , \tag{3.3}$$

which further complicate the relaxation formulas but are more convenient than cylindrical coordinates for three reasons. First, equipotentials of an ideal trap are transformed into straight lines parallel to the $\hat{s}$ axis. For a square mesh in (s,t) space as shown in Fig. 5, mesh points thus lie exactly along the endcap and ring electrodes. The calculation can thus proceed without fear of introducing errors due to mismodeling such boundaries, even for a coarse mesh. Second, owing to the choice of the coordinate s, mesh points lie along the $\hat{\rho}$ and $\hat{z}$ axes, so that these boundaries too are modeled exactly. Finally, the mesh density is much greater in the asymptotic region as can be seen in Fig. 6 which shows the resulting distribution of mesh points in the (ρ,z) plane. The greater density is needed in this region to model compensation electrodes of various shapes and to handle the variations of the potential which occur there. The near-rectangular structure of the transformed trap area shown in Fig. 5 is also very convenient for numerical bookkeeping.

Laplace's equation in the new coordinates has the form

$$0=\frac{\partial^2 V}{\partial s^2}+\frac{\partial^2 V}{\partial t^2}+f(s,t)\frac{\partial^2 V}{\partial s\,\partial t}+g(s,t)\frac{\partial V}{\partial s}\ , \tag{3.4}$$

where the functions f and g are defined by

$$f(s,t)=2(s+3t)/(3s+t)\ , \tag{3.5}$$

$$g(s,t)=4/(3s+t)\ . \tag{3.6}$$

Expressions for the various derivatives in Eq. (3.4) are derived to desired accuracies by simultaneously solving truncated Taylor series expansions for the potentials at neighboring mesh points. Substituting these in Laplace's equation produces the relaxation formula

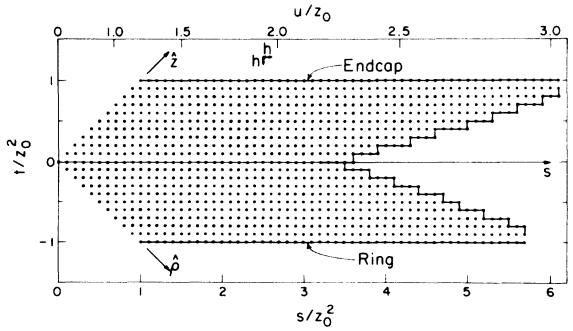

FIG. 5. Model Penning trap of Fig. 2 as it appears in (s,t) space following the transformation of Eqs. (3.2) and (3.3). Square mesh of side h is introduced for the relaxation calculation.

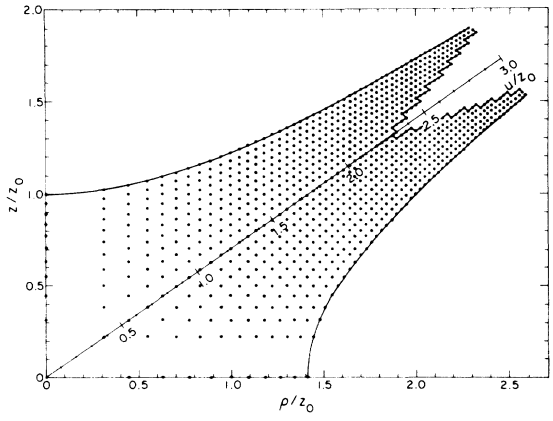

FIG. 6. Model Penning trap and the square mesh of Fig. 5 as they appear in (ρ,z) space. Relaxation calculation with this course mesh yields potential coefficients accurate to better than 5%. Mesh densities three to four times greater were used to achieve accuracies better than 1% in the low order C_k.

$$V_{0,0}=[\tfrac{1}{4}(V_{1,0}+V_{0,1}+V_{-1,0}+V_{0,-1})+\tfrac{1}{16}f(s,t)(V_{1,1}-V_{1,-1}-V_{-1,1}+V_{-1,-1})$$
$$+\tfrac{1}{24}g(s,t)h(V_{-2,0}+2V_{1,0}-6V_{-1,0})][1-\tfrac{1}{8}g(s,t)h]^{-1}\,. \tag{3.7}$$

The subscripts denote the relative position (in the $\hat{s}$ and $\hat{t}$ directions and in units of h) of the various potentials from the point of interest denoted by $V_{0,0}$. This relaxation formula has corrections of order h^4 which are neglected and is thus exact for Legendre polynomials P_k multiplied by r^k for $k=0$–6. Equation (3.7) is applied to all mesh points except those on and next to the $\hat{\rho}$ and $\hat{z}$ axes. Eight additional formulas of similar complexity with corrections of order h^3 or smaller are used for these points. A less convenient array of nearest mesh points is available for each of these points because of their proximity to the ρ and z axes. The appropriate axial and/or reflection symmetry is built into the relaxation formulas used on the axes. Each formula was tested numerically.

In each iteration, the relaxation formulas are used to recompute the potential at each mesh point in terms of its neighbors, beginning in the asymptotic region and moving toward the center of the trap. The boundaries are loaded as appropriate for ϕ_c and $\Delta\phi_0$, and the interior points are taken to be at zero potential for a starting estimate. Every 1000 iterations the potentials of the six points nearest the center of the trap are examined. Iterations are discontinued when the sum of these potentials converges to the full single precision (approximately seven significant figures) of a Floating Point Systems array processor hosted in a VAX computer. Since each electrode configuration required from 8000 to 28 000 iterations, taking from 1 to 10 h, it is indeed fortunate that this array processor was made available by the University of Washington Physics Department. The convergence criterion used is more stringent than is absolutely required, but it removes lack of convergence as a possible source of computational error. It was also unnecessary to develop techniques to accelerate convergence. The converged potentials at mesh points with $r/d<1$ are fitted (by linear least squares) to the appropriate small r/d expansion in even-order Legendre polynomials [Eq. (2.14) or (2.16)] truncated at $k=18$. The expansion coefficients so determined ($V_0 dC_k/dV_c$ and $C_k^{(0)}$ for ϕ_c and $\Delta\phi_0$, respectively) are plotted and discussed in the following sections.

The accuracies of the calculated potential coefficients are immediately tested by a second relaxation. This time new boundary potentials on the endcap, ring, and compensation electrode boundaries are determined from the appropriate expansion [in Eq. (2.14) or (2.16)] using the calculated expansion coefficients with $k\leq 18$. The time-consuming relaxation calculation is repeated, and another set of potential coefficients is extracted by least-squares fitting. The differences between the original expansion coefficients and these test coefficients are taken to be indications of uncertainties. By this test, the coefficients reported in this paper are accurate to better than 1% with a maximum mesh density three to four times greater than that shown in Figs. 5 and 6.

Finally, the dependence of the calculated quantities upon the mesh density was also investigated. Figure 7(a), for example, shows $V_0 dC_2/dV_c$ for an asymptotically symmetric trap as a function of the number of mesh intervals in $d=z_0$. The percent scale on the right indicates the $V_0 dC_2/dV_c$ has converged to within 1% for d divided into 40 mesh intervals. The ratios of tunabilities in Figs. 7(b) and 7(c) are converged ten times better.

IV. ASYMPTOTICALLY SYMMETRIC TRAPS

The endcap and ring electrodes of the traps used for the high-precision electron, positron, and proton experiments previously mentioned, all lie on hyperbolas as in Eqs. (2.1) and (2.2) with $\rho_0=\sqrt{2}z_0$. These hyperbolas are symmetric about the asymptote ($z^2=\frac{1}{2}\rho^2$) for large ρ and z. Because of the popularity of such asymptotically symmetric traps,

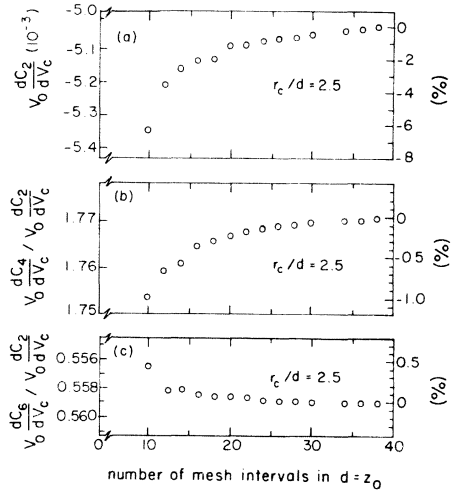

FIG. 7. Dependence of $V_0 dC_2/dV_c$ and two ratios of tunabilities upon the number of mesh intervals in d, for an asymptotically symmetric trap with $r_c/d=2.5$ and $\alpha=180°$. Percent scales on the right refer to the values obtained with 40 mesh intervals in d.

they are discussed initially in detail, using the model in Fig. 2. Comparisons of calculation and experiment provide tests of the calculation and the calculation in turn provides useful information for the experiments in progress which are using asymptotically symmetric traps.

An important feature of anharmonicity compensation is demonstrated in Fig. 8 where $V_0 dC_2/dV_c$ (the tunability for C_2) is plotted versus the normalized distance r_c/d from the center of the trap to the compensation electrode along the asymptote. Notice that the logarithmic vertical scale covers nearly seven orders of magnitude while r_c/d on the horizontal scale changes only by a factor of 4 and covers the range over which compensated, asymptotically symmetric traps have been built. The rapid falloff is due to the severe screening of the compensation potential by the endcap and ring electrodes. As is well known, the potential at a large distance r from a line of charge[16] or from a flat electrode[17] is reduced by a factor of $\exp(-\pi r/l)$ when grounded, perfectly conducting plates spaced a distance l apart are located as shown in Fig. 9(a) or 9(b), respectively. Locally, the slopes of the curves in Fig. 8 are approximately described by this exponential factor with $r = r_c$ and l taken to be the separation of the endcap and ring electrodes at $r = r_c$.

The solid line in Fig. 8 represents the tunability $V_0 dC_2/dV_c$ for flat compensation electrodes perpendicular to the asymptote ($\alpha = 180°$ in Fig. 2). The dashed line represents $\alpha = 30°$. These two choices are plotted to allow comparison with three available measured values. The comparison is encouraging considering that the traps are imperfectly modeled and especially considering the steep falloff with increasing r_c/d. For the proton trap (the smallest of the three traps in Fig. 8), a change in the location of the compensation electrode by only 250 μm would thus change $V_0 dC_2/dV_c$ by a factor of 3. Several other traps have been constructed which do not fit on Fig. 8 since $r_c/d > 4$. These traps could not be tuned to eliminate anharmonicities, because a large enough V_c/V_0 could not be applied.

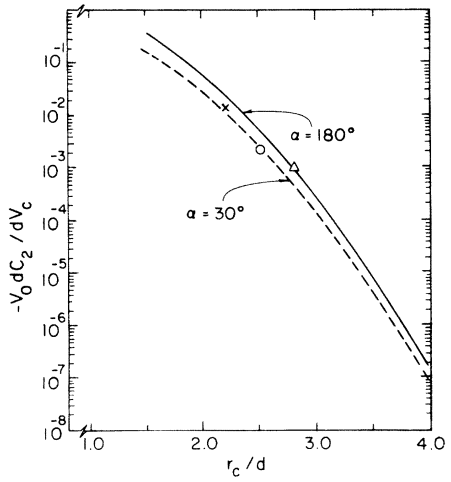

FIG. 8. Tunability $V_0 dC_2/dV_c$ for asymptotically symmetric, compensated Penning traps with $\alpha = 180°$ and 30°. Measured values are for the positron trap of Ref. 4 with $\alpha = 30°$ (×), the proton trap of Ref. 6 with $\alpha = 30°$ (○), and the electron trap of Fig. 1 with $\alpha = 180°$ (△).

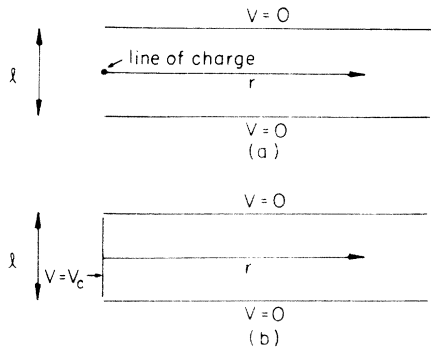

FIG. 9. Two-dimensional screening models. Parallel flat plate electrodes screen the potential produced (a) by a line of charge and (b) by a perpendicular electrode. In both cases, for $r_c \gg l$, a screening of the potentials by a factor of $\exp(-\pi r_c/l)$ results.

The strong electrostatic screening not only causes the rapid falloff of $V_0 dC_2/dV_c$ with increasing r_c/d but also completely shapes the potential which penetrates to the center of the trap. This observation is crucial to this paper and means that $V_0 dC_4/dV_c$ and $V_0 dC_6/dV_c$ are essentially proportional to $V_0 dC_2/dV_c$. In Fig. 10, the tunabilities for C_4, C_6, and C_8 are normalized to the tunability $V_0 dC_2/dV_c$ and are plotted versus the location of the compensation electrode r_c/d. The ratios (and hence the shape of the potential near the center of the trap) converge with increasing r_c/d to values which are strikingly independent of both the location of the compensation electrodes (represented by r_c/d) and the shape of the compensation electrode (as modeled by α). Even for compensation electrodes extending as far into the trap as $r_c/d = 1.5$, however, the dependence on the point angle of the compensation electrodes α is slight enough to allow plotting the ratios of tunabilities on a linear vertical scale (in Fig. 10), despite the fact that the tunabilities are individually changing by seven orders of magnitude over the range of r_c/d covered in this figure. For a particular r_c/d, changing from $\alpha = 180°$ to 0° reduces the tunabilities by roughly a factor of 2 (Fig. 11). The choice of α for the compensation electrode is, however, only important in-

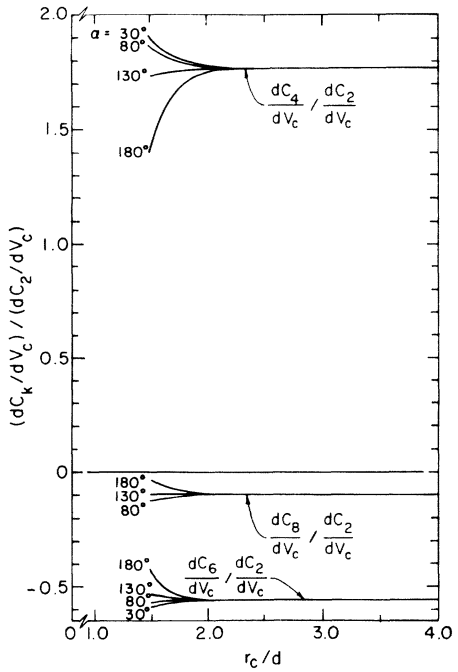

FIG. 10. Ratios of the tunabilities (as labeled) for asymptotically symmetric Penning traps. These ratios clearly approach a limit for $r_c/d > 2$ which is independent of both α and r_c/d. Tunabilities in these ratios vary individually by nearly seven orders of magnitude over the range of r_c/d plotted here.

sofar as it establishes an effective r_c/d for an equivalent flat compensation electrode.

The quality factor γ defined earlier [in Eqs. (2.19) and (2.20)] represents the undesirable change $\Delta\omega_z/\omega_z$ which accompanies a change ΔC_4 brought about by adjusting the compensation potential. Observe that γ is the inverse of the ratio of tunabilities plotted as the upper curve in Fig. 10. The successful compensated traps referred to earlier all have

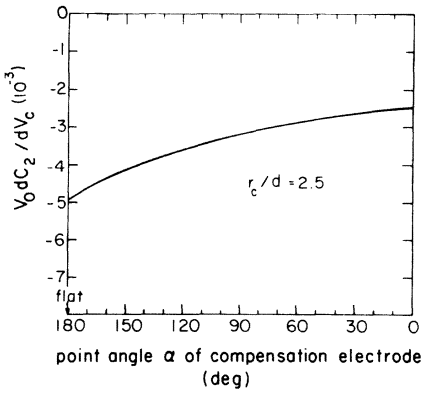

FIG. 11. Dependence of $V_0 dC_2/dV_c$ upon the point angle of the compensation electrodes for asymptotically symmetric, compensated Penning traps with $r_c/d = 2.5$.

$r_c/d > 2$ and thus share the same quality factor $\gamma \approx 0.56$ which is remarkably independent of the location and shape of the compensation electrode. Innovations in the shape and location of the compensation electrodes clearly have not and cannot improve the quality factor for asymptotically symmetric traps.

Knowledge of $V_0 dC_4/dV_c$ is very useful since it allows an adjustment of C_4 by a known amount to test for systematic effects of anharmonicity. The trap of Fig. 1 is well modeled (in Fig. 2) and in fact was designed using the results of this relaxation calculation. A value of $(d\omega_z/dV_c)/(d\omega_z/dV_0)$ equal to -10^{-3} is calculated and measured. The calculated value of $V_0 dC_4/dV_c$ of -2×10^{-3} suggests that a change in V_c/V_0 of approximately 5% is required to produce a change $\Delta C_4 \approx 10^{-4}$. For traps not well modeled in Fig. 2 the measurement of $(d\omega_z/dV_c)/(d\omega_z/dV_0)$ and the calculated value of γ must both be used. The first compensated trap, for example, has endcap and ring electrodes truncated at $r_c/d \approx 2.2$ (according to the scale drawing in Ref. 9). The compensation electrode is located back at $r_c/d \approx 2.7$ and is not symmetric about the asymptote. A value of $(d\omega_z/dV_c)/(d\omega_z/dV_0)$ equal to -3×10^{-3} is measured,[15] suggesting (from Fig. 8) that this trap has the properties of a trap with flat compensation electrodes at $r_c/d \approx 2.6$. A change in V_c/V_0 of approximately 2% is required to produce a change $\Delta C_4 \approx 10^{-4}$ according to Eq. (2.21). The insensitivity of γ to the shape and location of the compensation electrodes should make such a calibration reliable.

Figures 8, 10, and 11 provide a rather complete description of ϕ_c near the center of the asymptotically symmetric traps. Changes in C_2, C_4, C_6, and C_8 which occur when the compensation potential V_c is changed can be deduced from these figures. Agreement between the calculation and the few available measured values is very good. To complete the description of asymptotically symmetric traps, the relaxation calculation is also used to similarly calculate the solutions $\Delta\phi_0$ from which the coefficients $C_k^{(0)}$ are determined. Exact counterparts to Figs. 8 and 10 reveal the same steep dependence upon r_c/d shown in Fig. 8 and establish that the shape of $\Delta\phi_0$ near the center of the trap is also essentially independent of both α and r_c/d.

Detailed plots of the $C_k^{(0)}$ are much less useful than Figs. 8, 10, and 11 and thus are not included in this paper. The reason is that the calculated values of the $C_k^{(0)}$ are significantly modified by the addition of holes and slits in the quadrupole electrodes as well as by imperfections and misalignments of these electrodes. This occurs because the boundary conditions for ϕ_0 and hence $\Delta\phi_0$ are modified by these ad-

ditions. To illustrate, consider the ratios of $-C_4^{(0)}$ to $V_0 dC_4/dV_c$ plotted in Fig. 12. Equation (2.13) establishes that these ratios are equal to the values of the normalized compensation potential V_c/V_0 required to make C_4 vanish for flawless traps with no holes and slits in the electrodes. For flat compensation electrodes ($\alpha=180°$) the required V_c/V_0 is always less than a few percent. For $\alpha=30°$, the required values are even smaller, less than 0.5%. The small values were anticipated (in Sec. II) because the potential of the compensation boundary is more monopolelike for ϕ_c and more dipolelike for $\Delta\phi_0$, but should only be regarded, however, as limiting or reference values. Existing traps tune up at much larger values of $|V_c/V_0|$ ranging from -200% (trap in Fig. 1) to -10% (for the positron trap[4]) to 1000% (for the proton trap[6]).

V. AN OPTIMAL HYPERBOLIC PENNING TRAP

Essentially no progress has been previously made toward producing a trap with a smaller quality factor γ. The first compensated trap reported seven years ago and traps constructed last year all were asymptotically symmetric traps with γ close to the value $\gamma\approx 0.56$ which is independent of α and r_c/d. The relaxation calculation discussed earlier establishes clearly that attempts to reduce γ by changing the shape and location of the compensation electrodes were not successful because electrostatic screening determines the shape of the equipotentials for ϕ_c near the center of the trap, especially for $r_c/d>2$.

For an asymptotically symmetric trap, the endcap electrodes are closer to the center of the trap and to the asymptote than is the ring for $r<d$. The endcaps thus screen the compensation potential more strongly than does the ring. Equipotentials for ϕ_c which penetrate near the center of the trap thus are not symmetric about the asymptote $z^2=\frac{1}{2}\rho^2$, but are shifted lower in the trap. The quality factor γ will vanish only if the tunability $V_0 dC_2/dV_c$ vanishes. This tunability is the expansion coefficient which multiplies the second-order Legendre polynomial P_2 in the expansion (2.14) for ϕ_c. Since P_2 vanishes on the asymptote, the tunability for C_2 and hence γ will vanish if the equipotentials for ϕ_c are symmetric about the asymptote near the center of the trap. To reduce $|\gamma|$ it thus is apparent (once the dominant role of electrostatic screening is fully understood) that ρ_0 and z_0 must be made more nearly equal than in an asymptotically symmetric trap, to make ϕ_c as symmetric as possible about the asymptote.

The first computational search for the optimal symmetry, done for $r_c/d=2.5$, is summarized in Fig. 13. The tunabilities $V_0 dC_2/dV_c$ and $V_0 dC_4/dV_c$ are plotted as functions of $\frac{1}{2}\rho_0^2/z_0^2$ which ranges from $\frac{1}{2}$ to 1. The $\frac{1}{2}$ corresponds to $\rho_0=z_0$, and the 1 identifies an asymptotically symmetric trap (with $\rho_0=\sqrt{2}z_0$). (These configurations are not that much different from each other as may

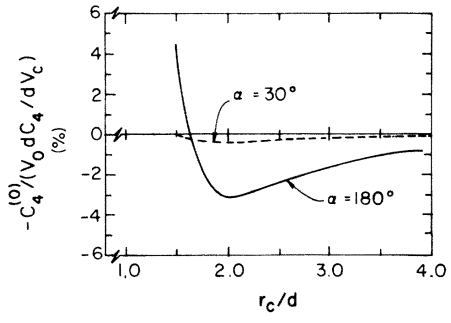

FIG. 12. Ratio of $-C_4^{(0)}$ to $V_0 dC_4/dV_c$ for asymptotically symmetric traps with $\alpha=30°$ and 180° as a function of r_c/d. For a perfectly aligned electrode with no holes, slits, or imperfections, the vertical scale is the normalized compensation potential V_c/V_0 required to make C_4 vanish.

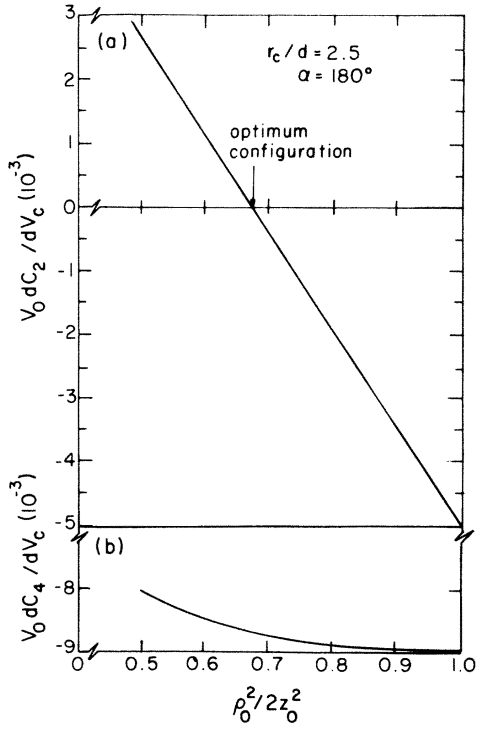

FIG. 13. Tunabilities (a) $V_0 dC_2/dV_c$ and (b) $V_0 dC_4/dV_c$ as functions of $\rho_0^2/2z_0^2$ for a trap with $r_c/d=2.5$ and $\alpha=180°$. Quality factor $\gamma=0$ at the point where $V_0 dC_2/dV_c$ vanishes.

be seen in Fig. 14, where the hyperbolas are pictured.) The tunability $V_0 dC_2/dV_c$ [in Fig. 13(a)] varies linearly with $\frac{1}{2}\rho_0^2/z_0^2$ going through zero at $\frac{1}{2}\rho_0^2/z_0^2 \approx 0.674$. By contrast, $V_0 dC_4/dV_c$ [in Fig. 13(b)] varies only slightly as might be expected, since P_4 varies only slightly near the asymptote. The quality factor γ is the ratio of the plotted tunabilities. It thus goes to the ideal value of $\gamma=0$ at the zero crossing point.

The relaxation calculation was used to make curves like those in Fig. 13 for different values of r_c/d. The value of $\frac{1}{2}\rho_0^2/z_0^2$ required to achieve $\gamma=0$ was determined from these curves and is plotted in Fig. 15 as a function of r_c/d. Notice that the optimum value of $\frac{1}{2}\rho_0^2/z_0^2$ changes by less than 3% for $r_c/d > 1.5$ and by only about 01.% for $r_c/d > 2$. The hyperbolas for the endcap and ring electrodes for an optimally designed trap with $r_c/d > 2$ are thus characterized by

$$\rho_0 \approx 1.16 z_0 \tag{5.1}$$

and are plotted in Fig. 14. The tunabilities $V_0 dC_4/dV_c$ and $V_0 dC_6/dV_c$ for such optimally designed traps are essentially the same for a particular r_c/d as those reported for asymptotically symmetric traps in Sec. IV and therefore can be obtained from Figs. 8 and 10.

In practice, of course, it will be impossible to achieve $\gamma=0$ because of imperfect mechanical tolerances. It seems likely, however, that $|\gamma|$ could be reduced by at least a factor of 20 from the $\gamma \approx 0.56$ currently being achieved with asymptotically symmetric traps. Such an improvement would make the tedious process of tuning out anharmonicities much easier and should facilitate the achievement of higher resolutions in ω_z as well.

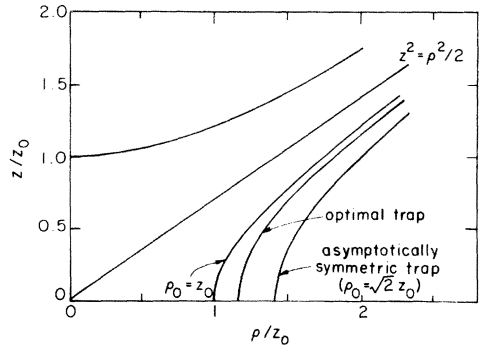

FIG. 14. Contours for the hyperbolic electrodes (from left to right) for a trap with $\rho_0=z_0$, an optimum trap, and an asymptotically symmetric trap. Endcap contour is shared by all three configurations.

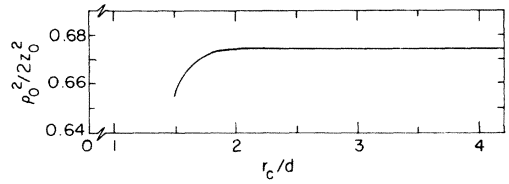

FIG. 15. Optimum value of $\rho_0^2/2z_0^2$ which makes $\gamma=0$, as a function of r_c/d for $\alpha=180°$. Optimal value rapidly approaches the limiting value ≈ 0.674 for $r_c/d > 2$.

VI. CONCLUSION

Two solutions to Laplace's equation, ϕ_c and $\Delta\phi_0$, completely determine the electrostatic potential in a compensated Penning trap for all trapping potentials (V_0), compensation potentials (V_c), and trap sizes (d). The boundary conditions for ϕ_c and $\Delta\phi_0$ are in Figs. 3(b) and 3(c). The key quantities for particle trapping are the lowest-order coefficients in small-r expansions of ϕ_c and $\Delta\phi_0$ because particles are typically trapped near the center of the trap. Thus the tunabilities $V_0 dC_2/dV_c$ and $V_0 dC_4/dV_c$ reveal the most important properties of ϕ_c, and $C_2^{(0)}$ and $C_4^{(0)}$ reveal the most important properties of $\Delta\phi_0$.

These expansion coefficients have been evaluated by a relaxation calculation for a variety of configurations of compensated Penning traps with hyperbolic endcap and ring electrodes. The coefficients are calculated for the model trap electrodes in Fig. 2 as a function of the location of the compensation electrodes (given by r_c/d), the shape of these electrodes (modeled by α), and as a function of the choice of hyperbolas (represented by ρ_0/z_0). The coefficients $C_2^{(0)}$ and $C_4^{(0)}$ are severely modified by the holes and slits in the hyperbolic electrodes of laboratory traps as well as by imperfections and misalignments. The calculated values of these coefficients thus must be regarded as limiting values to be approached in the limit of flawless electrodes. The tunabilities $V_0 dC_2/dV_c$ and $V_0 dC_4/dV_c$, fortunately, are much less affected by these additions, and the calculated values agree well with the measured values in the few cases they can be compared.

All of the existing high-precision compensated Penning traps have endcap and ring electrodes along hyperbolas with $\rho_0=\sqrt{2}z_0$ which symmetrically approach the quadrupole asymptotes for large ρ and z. Figures 8–12 reveal the important electrostatic properties of such asymptotically symmetric Penning traps. Not surprisingly, the potential of a compensation electrode is severely screened by the endcap and ring electrodes, the severity increasing for a compensation electrode farther from the center of

the trap. Thus Fig. 8 shows that $V_0 dC_2/dV_c$ decreases by more than six orders of magnitude between $r_c/d=1.5$ and $r_c/d=4.0$. Changing the shape of the compensation electrode can change the value of this coefficient by up to a factor of 2 (see, e.g., Fig. 11). The most striking result of the relaxation calculation, however, is that the shape of the compensation potential which penetrates to the center of the trap is essentially independent of the shape and location of the compensation electrode as is demonstrated in Fig. 10. The higher-order tunabilities $V_0 dC_k/dV_k$ are thus proportional to $V_0 dC_2/dV_c$ and have the same dependence on r_c/d and α.

The quality factor γ is defined [in Eqs. (2.19) and (2.20)] to quantify the undesirable fractional shift in the harmonic-oscillation frequency ω_z which accompanies a change in anharmonicity ΔC_4 brought about by tuning the compensation potential. The quality factor depends solely upon the shape of ϕ_c near the center of the trap. All of the past and present high-precision Penning traps thus have essentially identical quality factors ($\gamma \approx 0.56$) despite careful attention to asymptotic symmetry and despite innovations in the shape and location of compensation electrodes. Reducing the quality factor to the ideal value of $\gamma=0$ requires that equipotentials of the compensation potential ϕ_c at the center of the trap be made symmetric about the quadrupole asymptote. A major lesson from the relaxation calculation is that the shape of equipotentials of ϕ_c is determined by electrostatic screening by the endcap and ring electrodes and not by asymptotic symmetry. The quality factor can therefore be made to vanish only by a better choice of hyperbolas for the endcap and ring electrodes.

An optimal configuration of trap electrodes is proposed in Sec. V. At ρ_0/z_0 approximately equal to 1.16 the quality factor vanishes. This means that adjusting the compensation potential (to tune out anharmonicities) will, in principle, not change the harmonic-oscillation frequency ω_z of a trapped particle at all. Imperfect mechanical tolerances will of course prevent this ideal orthogonality from being realized, but an improvement over existing traps by a factor of 20 seems manageable. Optimally designed traps should be much more convenient to use and should facilitate the achievement of higher resolutions in the axial resonance frequency. In addition, the compensation electrodes in an optimally designed trap can be located nearer to the center of the trap. One advantage which results is that radio-frequency drives applied to these electrodes (to make $g-2$ transitions, for example) would be screened much less than in existing traps.

ACKNOWLEDGMENTS

I am grateful to H. Dehmelt for initially suggesting that I experimentally develop a trap design which minimized the undesirable dependence of the axial frequency on the compensation potential present in the currently used traps. When the alternative calculational approach reported here led me to propose the improved design of Sec. V, he was most encouraging. R. S. Van Dyck, Jr., graciously provided experimental information to supplement my own experience. This was very important for testing the calculation. L. S. Brown was helpful and supportive throughout and kindly provided the two-dimensional solution to Laplace's equation. Thanks are due to P. Schwinberg, P. Eckstrom, and D. Wineland for commenting on the manuscript. This work was supported by the National Science Foundation and by a Chaim Weizmann fellowship.

[1]D. Wineland, P. Ekstrom, and H. Dehmelt, Phys. Rev. Lett. 31, 1279 (1973).

[2]Reviewed in H. Dehmelt, *1982/83 McGraw-Hill Yearbook of Science and Technology* (McGraw-Hill, New York, 1982); P. Ekstrom and D. Wineland, Sci. Am. 243, 105 (1980).

[3]R. S. Van Dyck, Jr., P. B. Schwinberg, and H. Dehmelt, in *New Frontiers in High-Energy Physics,* edited by B. Kursuhoglu, A. Perlmutter, and L. Scott (Plenum, New York, 1978).

[4]P. B. Schwinberg, R. S. Van Dyck, Jr., and H. G. Dehmelt, Phys. Rev. Lett. 47, 1679 (1981).

[5]T. Kinoshita and W. B. Lindquist, Phys. Rev. Lett. 47, 1573 (1981).

[6]R. S. Van Dyck, Jr. and P. B. Schwinberg, Phys. Rev. Lett. 47, 396 (1981); R. S. Van Dyck, Jr. (private communication).

[7]G. Gabrielse and H. Dehmelt, in Proceedings of the Second International Conference on Precision Measurement and Fundamental Constants, Gaithersburg, 1981 (in press).

[8]H. Dehmelt (unpublished).

[9]R. S. Van Dyck, Jr., D. Wineland, P. Ekstrom, and H. Dehmelt, Appl. Phys. Lett. 28, 446 (1976).

[10]L. S. Brown and G. Gabrielse, Phys. Rev. A 25, 2423 (1982).

[11]Compensation electrodes could of course be located in other places than the asymptotic region. This original choice (Ref. 9), however, seems to be the best in general since it places more of the ring and endcaps near to the

center of the trap on equipotentials of the desired potential.

[12]One-dimensional anharmonic oscillators are discussed in L. D. Landau and E. M. Lifshitz, *Mechanics,* translated by J. B. Sykes and J. S. Bell (Pergamon, New York, 1976), pp. 87–89.

[13]Trap designed by F. Walls and reported in Ref. 9.

[14]Trap designed by G. Gabrielse and reported in Ref. 7.

[15]The first compensated trap was designed by P. Eckstrom. Pointed compensation electrodes were substituted in this design by R. S. Van Dyck, Jr., who kindly provided additional information beyond that reported in Ref. 9. For an axial temperature $T_z=26$ K, a well depth $qV_0=10$ eV, and an axial resonance frequency $\omega_z/2\pi=60$ MHz, an anharmonicity width $\Gamma_z/2\pi$ less than 1 Hz was observed. Thus $|\tilde{C}_4|<10^{-4}$. Probably $|\tilde{C}_4|$ was up to ten times smaller than this upper limit.

[16]L. S. Brown provided the solution to the two-dimensional problem in Fig. 9(a).

[17]H. Rothe and W. Kleen, *Hochvakuum-elektronenröhren I/Physikalische Grundlagen* (Akademische, Frankfurt 1955).